Food Bioengineering

WILEY

RESEARCH ARTICLE OPEN ACCESS

Engineering a Hybrid Heme Pathway for Hemoprotein-Based Dye-Decolorizing Peroxidase in *Escherichia coli*

Yue Sun[1,2] | Jin-Ping Chen[1,2] | Nan-Kai Wang[2,3,4] | Chang Su[1,2] | Heng Li[1,2] | Jin-Song Gong[1,2,5] | Zheng-Hong Xu[2,3,6] | Jin-Song Shi[1,2]

[1]School of Life Sciences and Health Engineering, Jiangnan University, Wuxi, Jiangsu, People's Republic of China | [2]Institute of Future Food Technology, JITRI, Yixing, Jiangsu, People's Republic of China | [3]National Engineering Research Center for Cereal Fermentation and Food Biomanufacturing, School of Biotechnology, Jiangnan University, Wuxi, Jiangsu, People's Republic of China | [4]Department of Engineering Science, University of Oxford, Oxford, Oxfordshire, UK | [5]Shandong Kunda Biotechnology Co., Ltd, Linyi, Shandong, People's Republic of China | [6]College of Biomass Science and Engineering, Sichuan University, Chengdu, Sichuan, People's Republic of China

Correspondence: Chang Su (emilysu1991@126.com) | Jin-Song Gong (jinsonggong.bio@hotmail.com)

Received: 19 March 2026 | **Revised:** 13 May 2026 | **Accepted:** 22 May 2026

Funding: National Key Research and Development Program of China, Grant/Award Number: 2024YFA0917900; Taishan Industry Leading Talent of Shandong Province, Grant/Award Number: tscx202408107; Key Laboratory of Carbohydrate Chemistry and Biotechnology of Ministry of Education, Grant/Award Number: KLCCB-KF202510

Keywords: aflatoxin B_1 degradation | dye-decolorizing peroxidase | *Escherichia coli* | heme biosynthesis | hemoprotein engineering

ABSTRACT

Dye-decolorizing peroxidases (DyPs) are heme-dependent oxidoreductases with promising applications in mycotoxin detoxification by acting on the oxidizable conjugated structures of aflatoxin B_1 (AFB_1). The heme prosthetic group is critical for the catalytic process by mediating electron transfer and intermediate formation that govern overall enzymatic activity. However, intracellular heme biosynthesis in microbial hosts is tightly regulated, frequently leading to suboptimal catalytic performance of recombinant DyPs, thus highlighting the necessity to improve cofactor availability. To establish an efficient heme-based expression system for DyPs, we developed a heme cofactor supplementation system in *Escherichia coli* by introducing a heterologous C4 pathway harboring 5-aminolevulinic acid synthase from *Caulobacter segnis* together with the outer membrane heme transporter ChuA. Furthermore, intracellular heme supply was optimized by the integrated overexpression of the C4 and C5 pathways as well as the *hemEFGH* gene cluster, which significantly enhanced *Rh*DypB-R80 activity. The engineered cells exhibited substantially higher heme content and *Rh*DypB-R80 activity compared to those produced by conventional cultivation methods supplemented with exogenous 5-ALA. Notably, heme-based *Rh*DypB-R80 achieved 91.03% AFB_1 degradation within 24 h, demonstrating its potential for enzymatic detoxification applications. This engineered heme-producing host provides a practical platform for enhancing hemoprotein activity and supports the development of enzymatic strategies for mycotoxin control in food systems.

1 | Introduction

Mycotoxins are low-molecular-weight secondary metabolites produced during the growth and reproduction of fungi (Mafe and Büsselberg 2024). There are currently over 500 known mycotoxins worldwide, among which the most relevant in feed are aflatoxin B_1 (AFB_1), ochratoxin A (OTA), fumonisin B_1 (FB_1), vomitoxin (DON), and zearalenone (ZEN) (Eskola et al. 2020). When ingested by humans and animals, they can cause a variety of diseases, including cancer, liver and kidney tumors, reproductive system disorders, and neural tube defects (Khan et al. 2024). Mycotoxins have become a pressing issue in the field of food safety due to their significant impact on human

and animal health and widespread global contamination. Notably, most mycotoxins exhibit strong heat resistance (Bullerman and Bianchini 2007), making them difficult to be degraded under conventional food processing temperatures. Therefore, the development of effective strategies for detoxification has emerged as an urgent priority in food safety research.

Biological detoxification strategies based on microorganisms and enzymes have attracted increasing attention as viable alternatives to traditional physical and chemical decontamination approaches. As opposed to these traditional procedures, enzymatic and microbial processes operate under mild physiological conditions and exhibit high specificity towards substrates (Diao et al. 2018; Xu et al. 2022). Efforts to find effective mycotoxin biocontrol have focused more on oxidoreductases, with peroxidases being especially promising (Wang et al. 2019). Though MnP from the white-rot fungus *Phanerochaete sordida* YK-624 has an 86% AFB_1 degradation rate (Wang et al. 2011), its reliance on Mn^{2+} as a redox mediator may complicate its use in a complex food system (Hofrichter 2002). In comparison, dye-decolorizing peroxidases (DyPs) are independent of metal mediators. For instance, immobilized *Rh*DypB exhibited 85.61% elimination efficiency of AFB_1 under identical reaction circumstances (Du et al. 2025). The catalytic action of DyPs relies on the correct insertion of the heme cofactor into the apoenzyme (Fiege et al. 2018). Structurally, bacterial DyPs are distinct from classical heme peroxidases, possessing a ferredoxin-like fold that sequesters heme within a buried hydrophobic pocket (Zámocký et al. 2015). In this active site, the heme iron is bound by a highly conserved proximal histidine (His), and the distal portion contains conserved aspartate (Asp) and arginine (Arg) catalytic residues (Sugano et al. 2007). Access to this concealed redox center is donated by particular solvent channels: one of which is involved in the entry of H_2O_2 (Strittmatter et al. 2013) and an internal cavity that facilitates the passage of electrons through the substrate (Pfanzagl et al. 2019). This arrangement permits the ferric enzyme to be oxidized through H_2O_2 to the $[Fe^{IV} = O\ Por\cdot]^+$ intermediate (compound I). Repeated one-electronreductions by the substrate produce compound II and ultimately restore the resting state of Fe^{III} (Roberts et al. 2011). Recent studies show that this process allows DypB to directly attack the electron-rich furan ring of AFB_1, in effect transforming the toxin into less mutagenic analogs (Loi et al. 2020). These structural features form the basis of the catalytic versatility of the enzyme discussed in this research.

Escherichia coli serves as a predominant host for producing recombinant enzymes. However, for hemoprotein-based biocatalysis of DyPs, this recombinant expression system still requires further optimization to facilitate the practical application in mycotoxin degradation (Hu et al. 2023). This is largely due to the strict regulation of heme biosynthesis in host organisms, which often results in the accumulation of inactive apoenzymes when recombinant hemoproteins are overexpressed. The exogenous addition of protohemin or 5-aminolevulinic acid (5-ALA, an intermediate in the heme synthesis pathway) into culture media is known to partially enhance the production of holoenzymes (Yu et al. 2024). However, the high cost of protohemin and 5-ALA poses a significant challenge for the practical applications of hemoprotein-based biocatalysis. In addition, enzymes developed for aflatoxin B_1 detoxification must be suitable for food and feed systems, where endotoxin contamination from conventional *E. coli* strains is undesirable. To address this issue, we explored metabolic engineering of the heme biosynthetic pathway in a low-endotoxin *E. coli* strain, aiming to enable efficient recombinant expression of active mycotoxin-degrading enzymes.

In this study, a heme-producing *Escherichia coli* strain was constructed as a microbial chassis for dye-decolorizing peroxidase (*Rh*DypB) expression. The heme biosynthetic pathway was reconstructed by introducing the heterologous C4 pathway for 5-aminolevulinic acid (5-ALA) synthesis and simultaneously enhancing the endogenous pathways for 5-ALA and uroporphyrinogen III (urogen III) production. Moreover, genomic engineering was used to streamline the downstream biosynthetic pathway, identifying key rate-limiting factors and facilitating the construction of high-yielding strains. The resulting recombinant strain was used to express the dye-decolorizing peroxidase. This reconstituted heme-binding enzyme had better efficacy in aflatoxin B_1 (AFB_1) degradation and showed increased thermal stability in comparison to its apoenzyme counterpart. Molecular dynamics simulation revealed that AFB_1 degradation is driven primarily by hydrophobic and polar interactions between the substrate and *Rh*DypB. Collectively, this work presents a novel strategy for the efficient expression and application of mycotoxin-degrading enzymes.

2 | Materials and Methods

2.1 | Strains, Media, and Growth Conditions

The primers listed in Supporting Information S1: Table S1 were synthesized by GENEWIZ Biotechnology (Suzhou, China). The complete list of strains used and constructed in this study is presented in Supporting Information S1: Table S2. An engineered *E. coli* BL21(DE3)-derived strain, ETF13, previously developed in our laboratory, was used as the host for plasmid propagation and heterologous protein expression. ETF13 carries deletions in genes associated with lipopolysaccharide core, O-antigen, capsule biosynthesis, and lipid A modification pathways. The relevant deletion genotype is provided in Supporting Information S1: Table S2. Routine cloning and liquid cultivation of *E. coli* strains were performed using Lysogeny Broth (LB) medium. Antibiotics were used at the following final concentrations: 50 $\mu g \cdot mL^{-1}$ kanamycin sulfate, 50 $\mu g \cdot mL^{-1}$ streptomycin sulfate, 34 $\mu g \cdot mL^{-1}$ chloramphenicol, and 100 $\mu g \cdot mL^{-1}$ ampicillin.

The following reagents were obtained from commercial suppliers: 2,2′-azino-bis(3-ethylbenzothiazoline-6-sulfonic acid) (ABTS) from Yuanye Bio-Technology (Shanghai, China), methanol and 5-aminolevulinic acid (5-ALA) from Adamas-beta (Shanghai, China), aflatoxin B_1 from Chengdu Alfa Biotechnology (Chengdu, China), and hemin from Macklin Biochemical (Shanghai, China). Protein markers, protein loading buffers, and PAGE gel preparation kits were purchased from Yeasen Biotechnology (Shanghai, China).

2.2 | Heterologous Expression and Purification of Recombinant *Rh*DypB

The recombinant strain expressing *Rh*DypB was initially grown in 10 mL of LB medium supplemented with 50 μg·mL^{-1} kanamycin sulfate at 37°C with shaking for 12 h. This seed culture was then transferred at a 1% (v/v) inoculum into 50 mL of fresh LB medium containing the same antibiotic concentration. When the optical density at 600 nm (OD_{600}) reached 1.0, protein expression was induced by adding isopropyl β-D-1-thiogalactopyranoside (IPTG) to a final concentration of 0.5 mmol·L^{-1} along with 25 mg·L^{-1} hemin. The culture was subsequently incubated at 25°C for 12 h.

After cultivation, cells were harvested by centrifugation at 8000 rpm for 10 min at 4°C. The pellet was resuspended in 25 mmol·L^{-1} Tris-HCl buffer (pH 7.8) containing 0.3 mol·L^{-1} NaCl and disrupted by sonication on ice with 2 s pulses intervals and 3 s intervals for 20 min. The lysate was clarified by centrifugation at 8000 rpm for 10 min at 4°C. The resulting supernatant was filtered through a 0.45 μm membrane to obtain the crude enzyme solution. Protein purification was carried out using a Ni-NTA affinity column. The column was washed with buffer containing 15 mmol·L^{-1} imidazole to remove non-specifically bound proteins, and the target protein was eluted with buffer containing 300 mmol·L^{-1} imidazole. The purified fraction was stored at 4°C for further analysis. The purified enzyme yield was calculated from the protein concentration of the purified fraction and the final elution volume and expressed as milligrams of purified protein per liter of culture.

2.3 | Engineering of Heme Transport Protein

Heme-related strains were generated by electroporating recombinant plasmids encoding heme transport proteins into electrocompetent cells harboring the *Rh*DypB-R80 expression plasmid. Transformants were selected on LB agar containing kanamycin (50 μg·mL^{-1}) and ampicillin (100 μg·mL^{-1}). A single colony was picked and inoculated into 10 mL of LB with the same antibiotics for 12 h, and 1% (v/v) of the culture was transferred into 50 mL of fresh LB medium. When the OD_{600} reached approximately 1.0, IPTG (0.5 mM) and tetracycline (1 mg·L^{-1}) were added to induce expression, followed by incubation overnight at 25°C.

To enhance heme uptake capability, the *chuA* (Fiege et al. 2018) gene from *E. coli* Nissle 1917 (NCBI accession: WP_000089583.1) and the *phuR* (Marvig et al. 2014) gene from *Pseudomonas aeruginosa* (NCBI accession: AAC13289.1) were amplified by PCR. The resulting amplification products were digested with specific restriction enzymes and subsequently ligated into the pTet2 vector. Detailed information on all constructed plasmids related to heme uptake is provided in Supporting Information S1: Table S3.

2.4 | Construction of the Heme Biosynthesis Pathway

Heme-producing strains were constructed by overexpressing genes from the heterologous C4 pathway, the endogenous C5 pathway, and downstream heme biosynthetic enzymes. For the C4 pathway, the genes encoding 5-aminolevulinic acid synthase (ALAS) from *Bradyrhizobium diazoefficiens* (BdALAS, UniProt ID: P08262), *Paracoccus denitrificans* (PdALAS, P43089), and *Caulobacter segnis* (CsALAS, D5VJ52) were PCR-amplified (Kato et al. 2025) and cloned into pTet2, pCDF, or pACYC vectors. The native C5 pathway and downstream flux were reinforced by amplifying key genes from *E. coli* BL21(DE3) genomic DNA. These genes included glutamyl-tRNA reductase (*hemA*) (Harnastai et al. 2006), glutamate-1-semialdehyde-2,1-aminomutase (*hemL*), and the subsequent enzymes in the pathway (*hemB*, *hemC*, *hemD*, *hemE*, *hemF*, *hemG*, and *hemH* (Ge et al. 2023). Detailed information on all constructed plasmids related to heme biosynthesis is provided in Supporting Information S1: Table S3.

2.5 | Determination of DyP Enzyme Activity

*Rh*DypB activity was assayed by monitoring ABTS oxidation at 420 nm. The standard reaction mixture contained 50 mM malonate buffer (pH 5.0), 1 mM ABTS, 1 mM $MnSO_4$, and 0.1 mM H_2O_2. Reactions were carried out at 25°C for 3 min, and activity was calculated from the initial increase in absorbance at 420 nm using $\varepsilon_{420} = 36000\ M^{-1}\cdot cm^{-1}$ for oxidized ABTS. One unit of activity was defined as the amount of enzyme required to generate 1 μmol of oxidation product per minute. For crude enzyme extracts, activity was expressed as volumetric activity in U·mL^{-1}, representing enzyme units per milliliter of crude extract. For purified enzyme samples, activity was normalized to protein concentration and expressed as specific activity in U·mg^{-1}. Protein concentration was determined using the BCA method.

2.6 | Optimization of Catalytic Conditions

The optimal conditions for *Rh*DypB-catalyzed ABTS oxidation were evaluated by varying pH, temperature, Mn^{2+}, and H_2O_2 concentrations. Enzyme activity was measured across a pH range of 3.0–8.0, temperatures from 15°C to 90°C, H_2O_2 concentrations of 0.05–2.0 mM, and Mn^{2+} concentrations of 0–1.0 mM.

2.7 | Degradation of AFB_1 by DyP

Mycotoxin degradation was carried out in a 50 mM malonate buffer solution at pH 5.0. The reaction system contained purified DyP at an enzyme dosage of 0.5 U·mL^{-1}, 0.6 mM $MnSO_4$, 0.2 mM H_2O_2, and AFB_1 at 2.5 μg·mL^{-1}. The reaction was performed at 20°C for 24 h. Three volumes of methanol were added to terminate the reaction, and the mixture was filtered through a 0.22 μm organic filter (Wang et al. 2019). Residual mycotoxin levels were quantified using an Agilent liquid chromatograph (Agilent Technologies Inc., California, USA). All experiments were conducted in triplicate.

2.8 | Molecular Docking and MD Simulations of the DyP–AFB_1 Interaction

Prediction of the tertiary structure of proteins was done using the SWISS-MODEL (https://swissmodel.expasy.org/interactive)

online server. The workflow was initiated by inputting the prepared protein sequence followed by automatic template search. Templates having high similarities (usually over 50%) were chosen to be used as the homology modeling basis. The optimal model was then selected based on Ramachandran plot analysis.

Molecular docking experiments were performed using AutoDock Vina (v1.2.3). Before docking, the three-dimensional structure of AFB_1 was retrieved from the PubChem database. Ligand and receptor preprocessing was conducted using AutoDock Tools software (v1.5.6), and the appropriate binding pocket was defined to produce the required configuration files. Continuous local search and repeated iteration using AutoDock Vina software was then done to determine the optimal molecular docking conformation. Result analysis and visualization were performed with the help of PyMOL (v4.6.0).

GROMACS 2024 was used to perform molecular dynamics (MD) simulations of the protein-small molecule system (AFB_1). Geometry optimization of the small-molecule ligand was performed using Gaussian 16. The protein-small molecule complex was centrally positioned within a cubic box, with the solute maintained at a distance of 1.0 nm from the box edges. The model was solvated using the SPC (Simple Point Charge) water model, and appropriate amounts of sodium and chloride ions were added to ensure the system's electroneutrality. Subsequently, the system was subjected to equilibration in the canonical (NVT) ensemble, where it was heated from 0 to 300 K, followed by equilibration at 300 K and 1 bar in an isothermal-isobaric (NPT) ensemble. A 200 ns molecular dynamics simulation of the protein-small molecule complex was performed, and simulation trajectories were saved for subsequent analysis. The MD results simulation were analyzed using metrics such as root-mean-square deviation (RMSD), radius of gyration (Rg), hydrogen bonds (H-bonds), and root-mean-square fluctuation (RMSF).

2.9 | Pyridine Hemochromogen Assay

The *E. coli* cells expressing hemoproteins (from a 45 mL culture) were centrifuged at 8000 rpm and 4°C, and then resuspended in 5 mL of Tris-HCl buffer (25 mM Tris-HCl, 300 mM NaCl, pH 7.8). The cells were disrupted by ultrasonic homogenization (amplitude: 30%, total processing time: 10 min, pulse-on: 2 s, pulse-off: 3 s), and the resulting lysates were centrifuged at 8000 rpm and 4°C for 10 min. The supernatants were then transferred to another tube. Next, the supernatants (0.50 mL) were mixed with 0.50 mL of potassium ferricyanide solution (500 μM $K_3[Fe(CN)_6]$ in 0.2 M aqueous NaOH containing 40% (v/v) pyridine), and the absorbance was recorded at 540 nm. The oxidized samples were subsequently treated with 10 μL sodium dithionite solution (0.5 M $Na_2S_2O_4$ in 0.5 M aqueous NaOH), and the absorbance was recorded at 557 nm. The concentration of pyridine hemochromogen in the sample was calculated from the difference between the absorbance at 557 nm of the reduced sample and the absorbance at 540 nm of the oxidized sample ($\Delta\varepsilon = 23.98\ mM^{-1}\cdot cm^{-1}$) according to the literature (Barr and Guo 2015). The heme-to-protein molar ratio of purified protein was calculated from the measured heme concentration and purified protein concentration to estimate the heme incorporation level.

2.10 | Statistical Analysis

All experiments were independently performed at least three times, and data are presented as the mean ± SD. Statistical data analysis was performed by two-tailedStudent's *t*-test in Excel (Microsoft Office 365). A threshold of $p < 0.05$ was set as the criterion for statistical significance, with asterisks denoting $^*p < 0.05$, $^{**}p < 0.01$, and $^{***}p < 0.001$.

3 | Results and Discussion

3.1 | Effect of Heme Cofactor on Activity and Stability of Peroxidase *Rh*DypB

Dye-decolorizing peroxidases (DyPs) comprise a recently discovered family of heme peroxidases with considerable biotechnological potential for degrading mycotoxins and lignin (Singh et al. 2013). *Rh*DypB from *Rhodococcus jostii* RHA1 is a heme-dependent DyP enzyme whose recombinant production may be limited by intracellular heme availability.

To verify this hypothesis, wild-type *Rh*DypB, hereafter referred to as *Rh*DypB^{WT}, and its soluble variant *Rh*DypB-R80 (Supporting Information S1: Table S4) were selected as model proteins to evaluate the effect of heme cofactor on peroxidase activity and stability (Supporting Information S1: Figure S1a,b). *Rh*DypB-R80 denotes a soluble *Rh*DypB^{WT} variant harboring the amino acid substitutions K84R, A115D, E160D, T200A, and L342P. Exogenous hemin at a final concentration of 25 $mg\cdot L^{-1}$ was added to the culture medium to supplement necessary cofactor. The purity of Ni-NTA-purified *Rh*DypB-R80 was confirmed by SDS-PAGE, and the purified enzyme yield was approximately 362 $mg\cdot L^{-1}$ of culture (Supporting Information S1: Figure S1c). The results showed that purified *Rh*DypB enzyme with heme exhibited significantly higher peroxidase activity compared to its apoenzyme form. Upon exogenous heme supplementation, the specific activities of *Rh*DypB^{WT} and the *Rh*DypB-R80 mutant increased by 2.52-fold and 2.82-fold, respectively (Figure 1a,b). Notably, residual peroxidase activity was observed in the absence of exogenous heme, attributable to low-level endogenous heme biosynthesis in *E. coli*. Given that thermostability is a crucial determinant of enzymatic practicality, we further characterized the thermodynamic properties of the enzymes across a temperature gradient. Distinct thermal profiles were observed: the peroxidase activity of *Rh*DypB decreased with increasing temperature without heme, while *Rh*DypB^{WT} and *Rh*DypB-R80 reached their highest peroxidase activities at 30°C in the heme-containing system. To corroborate these findings, we performed a Tm value determination using an SDS-PAGE-based thermal shift assay. *Rh*DypB^{WT} and *Rh*DypB-R80 were incubated at varying temperatures (0°C to 90°C) for 3 min, and then the retained soluble protein was quantified. As expected, the retained soluble proteins decreased with increasing temperature. At 40°C, *Rh*DypB^{WT} and *Rh*DypB-R80 retained less than 40% soluble protein, and nearly complete precipitation occurred at 60°C. However, residual catalytic

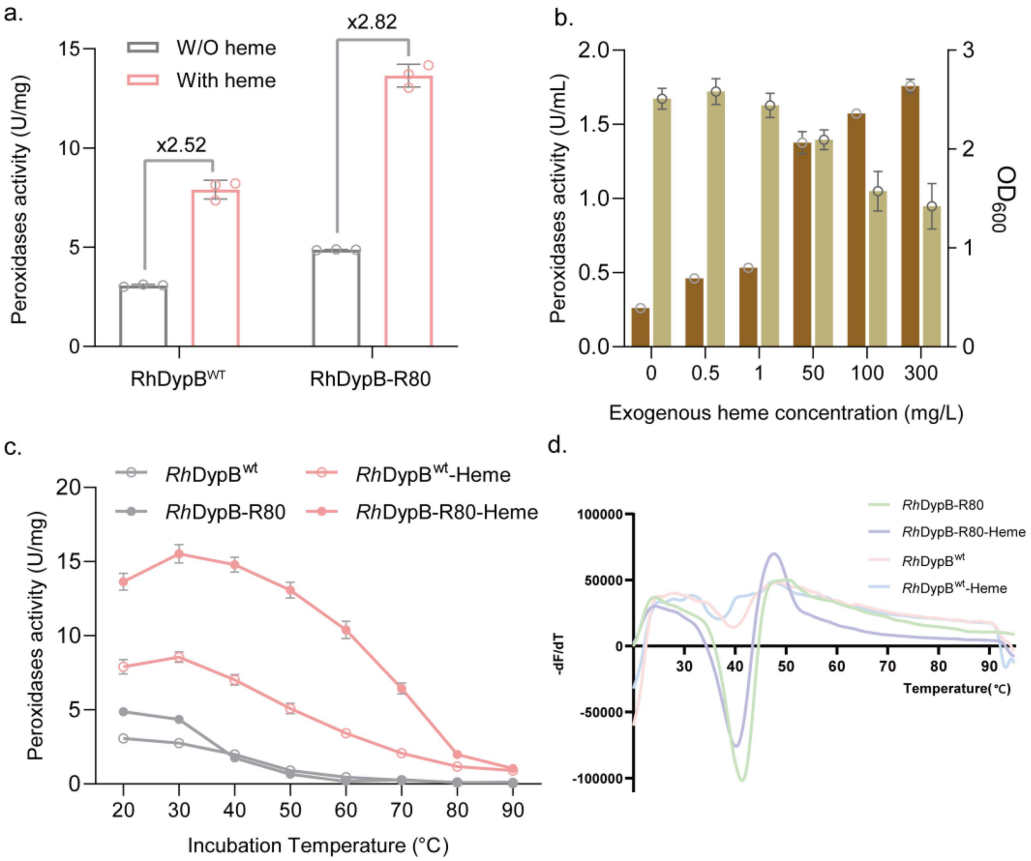

FIGURE 1 | Effect of exogenous heme addition on the enzymatic parameters of *Rh*DypB^{WT} and its mutant. (a) Impact of heme on peroxidase activity of *Rh*DypB and its mutant. (b) The effect of heme concentration on *Rh*DypB-R80 peroxidase activity. (c) SDS-PAGE-based thermal shift analysis of *Rh*DypB peroxidase. (d) Tm determination of enzymes using the SYPRO Orange probe-based thermal shift assay. The temperature at the lowest point of the curve represents the Tm value. Data are presented as the mean ± SD ($n = 3$).

activity was detectable even after incubation at 90°C (Figure 1c), suggesting that a minor fraction of the heme-bound enzyme retains structural integrity or that the heme moiety itself confers exceptional stability under extreme conditions. Furthermore, the Tm trends derived from the thermal shift assay were consistent with those obtained using the SYPRO Orange probe (Figure 1d). Collectively, these data indicate that heme binding substantially enhances the thermal robustness of the peroxidase.

3.2 | Transporter Engineering to Enhance Exogenous Heme Supply

Heme supplementation is a common practice to boost biocatalysis, but it is often constrained by the lack of efficient outer membrane transport machinery. To supply a suitable transporter for *Rh*DypB-R80, the genes encoding heme transporters, *phuR* from *P. aeruginosa* (Marvig et al. 2014) and *chuA* from *E. coli* Nissle 1917 (Fiege et al. 2018), were individually co-expressed with *Rh*DypB-R80. Intracellular heme content was quantified via the pyridine hemochromogen assay (Barr and Guo 2015) to evaluate heme uptake efficiency in each recombinant strain. ChuA overexpression significantly enhanced heme uptake with a 1.51-fold rise in intracellular heme content, leading to a 1.3-fold increased enzyme activity compared to the control (Figure 2a). In contrast, overexpression of the *phuR* gene reduced enzyme activity and heme content to 0.77-fold and 0.95-fold of the control levels, respectively. As outer membrane heme transporters, both transporters facilitate heme translocation into the periplasm, followed by cytoplasmic delivery via ABC transporters (Figure 2b; Chan et al. 2006). However, this process relies on specific interactions with the host TonB complex for energy transduction. The poor performance of PhuR is likely attributable to the interspecies incompatibility between the *Pseudomonas*-derived transporter and the *E. coli* TonB machinery, whereas the native ChuA couples efficiently (Noinaj et al. 2010). These results demonstrate that heterologous expression of heme transporter protein ChuA effectively enhances extracellular heme uptake. Therefore, *chuA* overexpression was used in subsequent strain construction.

The downstream conversion of PPIX to heme is strictly dependent on intracellular iron levels (Pranawidjaja et al. 2015). In *E. coli*, ferric iron acquisition is a complex process: it begins with the binding of Fe^{3+}-siderophore complexes to outer membrane receptors, followed by translocation into the cytoplasm via the TonB-ExbB-ExbD energy-transducing system and ABC-type transporters, where iron is finally released (Andrews et al. 2003). Based on this mechanism, Fe^{3+} was added at 0.5 mg·L^{-1} in the initial exponential growth stage. In this state, intracellular heme rose from 25.86 to 26.26 μmol·L^{-1} and *Rh*DypB-R80 activity rose from 0.69 to 0.79 U·mL^{-1}, a 1.16-fold

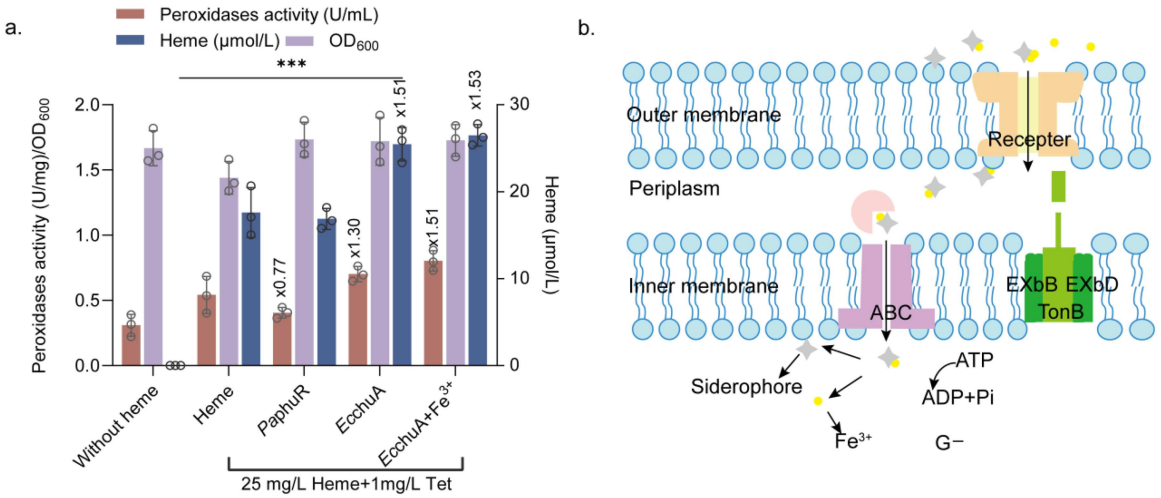

FIGURE 2 | Transporter engineering for enhancing heme content in *Escherichia coli* through exogenous heme uptake. (a) Heme concentration, enzymatic activity, and bacterial cell density in the supernatant of *E. coli*ETF13 cell lysates expressing *Rh*DypB-R80 via exogenous engineering. Data are presented as the mean ± SD ($n = 3$). Significance levels are indicated as follows: *$p < 0.05$, **$p < 0.01$, and ***$p < 0.001$. (b) Schematic diagram of the siderophore transport system in Gram-negative bacteria (G−).

enhancement compared to the *chuA*-only overexpression strain (Figure 2a). These findings indicate that Fe^{3+} supplementation at this given concentration is effective in promoting efficient heme biosynthesis.

3.3 | Improving Heme Supply by Enhancing the Endogenous Biosynthetic Pathway

ChuA-mediated transport confirmed the cofactor dependence of *Rh*DypB-R80, yet reliance on supplementation with exogenous heme was still restricted by limited membrane uptake and transporter capacity. We next increased intracellular heme supply by enhancing endogenous biosynthesis. Heme biosynthesis depends on 5-aminolevulinic acid (5-ALA), which is synthesized via the C4 and C5 pathways (Figure 3a; Ko et al. 2021; Layer 2021). The C4 pathway utilizes 5-aminolevulinic acid synthase (ALAS) to catalyze the condensation of succinyl-CoA and glycine into the heme precursor, 5-ALA. Unlike the native C5 pathway, which is tightly regulated by feedback inhibition, the heterologous C4 pathway functions independently of these regulatory mechanisms. Previous studies have shown that ALAS expression increases cellular 5-ALA levels and promotes heme accumulation in engineered *E. coli*. Therefore, ALAS was co-expressed with *Rh*DypB-R80 to improve heme incorporation into the recombinant enzyme.

Three ALAS genes from different organisms (Supporting Information S1: Table S5) were cloned into a tetracycline-inducible plasmid (termed pTet2) and co-expressed with pET-28a-*Rh*DypB-R80 (Pérez-Pérez and Gutiérrez 1995). Parallel cultures supplemented with exogenous 5-ALA were used as a control in the evaluation of peroxidase activity and intracellular heme titers. Despite the slight inhibition of cell growth during the dual-antibiotic selection, the introduction of all three ALAS homologs resulted in a significant increase in enzyme activity. The highest activity was observed with the strain that expressed CsALAS (0.485 U·mL^{-1}) which was a 51.5% increase compared to the control strain (0.32 U·mL^{-1}). The pyridine hemochromogen assay confirmed that the CsALAS-driven C4 pathway increased intracellular heme levels by 3.66-fold, reaching 1.84 μmol·L^{-1} (Figure 3b). Compared with exogenous 5-ALA feeding, CsALAS overexpression resulted in higher heme content and enzyme activity, possibly because rapid uptake of external 5-ALA can generate excess porphyrin intermediates and associated cytotoxic stress (Zhang et al. 2015).

During the 48 h fermentation, intracellular heme concentration and *Rh*DypB-R80 activity were measured. Heme concentration increased during early growth, reaching a maximum at 24 h (1.84 μmol·L^{-1}), and then gradually declined at 36 and 48 h. A similar trend was observed for enzyme activity, indicating that *Rh*DypB-R80 performance depends on intracellular heme availability (Figure 3c). To guide vector selection for subsequent heme-pathway engineering, we first compared CsALAS expression using three plasmid systems with different copy-number characteristics, including pTet2 (high-copy), pCDF (medium-copy), and pACYC (low-copy), using intracellular heme content and *Rh*DypB-R80 activity as evaluation criteria. Pyridine hemochromogen assays showed that the pTet2-based system produced the highest intracellular heme level, whereas the pCDF-based system yielded highest *Rh*DypB-R80 activity (Figure 3d). *Rh*DypB-R80 activity is expected to depend not only on intracellular heme availability but also on functional protein expression and heme incorporation. Therefore, pCDF was selected for subsequent pathway construction based on the higher *Rh*DypB-R80 activity observed in this system, and both intracellular heme levels and enzyme activity were assessed after 24 h fermentation.

In addition to the heterologous C4 pathway, the native C5 pathway was also strengthened to further increase intracellular heme levels and enzyme activity. In *E. coli*, the genes *hemA* and *hemL* are widely regarded as major control nodes in 5-aminolevulinic acid production, and several reports have demonstrated that their overexpression redirects carbon flux toward tetrapyrrole biosynthesis, resulting in improved heme

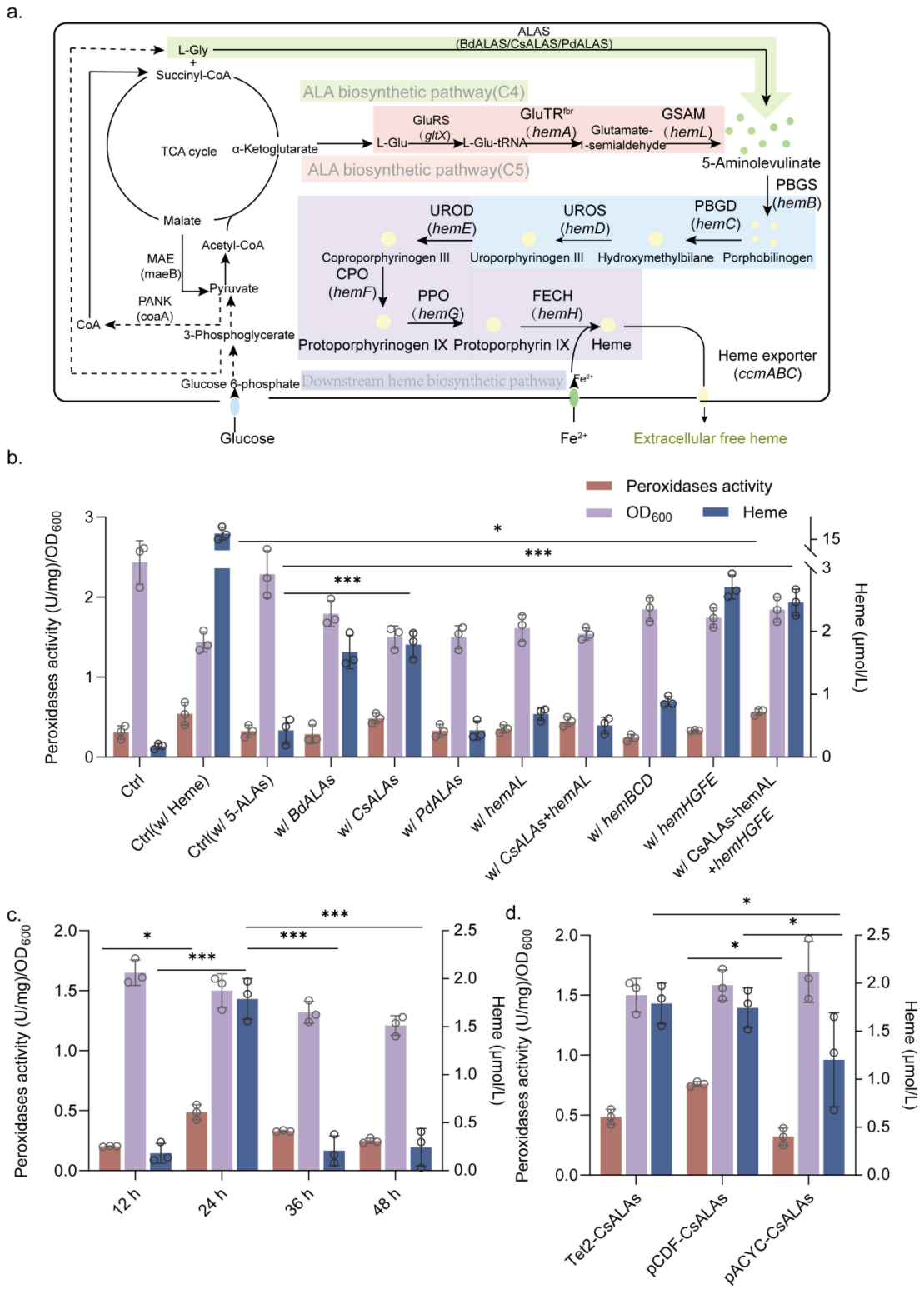

FIGURE 3 | Engineering strategies for optimizing heme production in *Escherichia coli*. (a) Heme biosynthetic pathways examined for secretory production of free heme. Metabolic pathways shaded in green, pink, blue, and purple represent the C4 pathway for ALA biosynthesis, the C5 pathway for ALA biosynthesis, and the downstream heme synthesis routes via the uroporphyrinogen III synthesis module and protoporphyrin IX synthesis module, respectively. In the final recombinant *E. coli* strain constructed in this study, pathways with overexpressed metabolic genes for heme secretion are indicated with bold arrows. Solid arrows denote single-step reactions, and dashed arrows represent multi-step processes. (b) Heme concentration, enzymatic activity, and bacterial cell density in the supernatant of *E. coli* ETF13 cell lysates expressing *Rh*DypB-R80-CsALAS via an optimized endogenous biosynthetic pathway. (c) Heme concentration, enzymatic activity, and bacterial cell density in the supernatant of *E. coli*-ETF13 cell lysates expressing *Rh*DypB-R80-CsALAS at different time points. (d) Heme concentration, enzymatic activity, and bacterial cell density in the supernatant of *E. coli*-ETF13 cell lysates expressing *Rh*DypB-R80-CsALAS using different vectors. Data are presented as the mean ± SD from three independent biological replicates. Significance levels are indicated as follows: $*p < 0.05$, $**p < 0.01$, and $***p < 0.001$.

formation (Mota et al. 2024). Consistent with previous reports, increasing *hemA* and *hemL* expression enhanced *Rh*DypB-R80 activity and raised intracellular heme content when compared with the strain receiving external 5-ALA supplementation. Even so, the magnitude of improvement was limited, and the heme level obtained through C5 pathway reinforcement remained clearly lower than that achieved by CsALAS-driven C4 pathway expression. Given the improvements obtained with individual pathway engineering, we next explored whether co-activation of the C4 and C5 pathways could produce a synergistic effect. A strain co-expressing CsALAS together with *hemA* and *hemL* was constructed. Contrary to expectation, simultaneous activation of the C4 and C5 pathways did not lead to higher heme accumulation. As shown in Figure 3b, intracellular heme levels in the combinatorial strain were lower than those observed in strains overexpressing either the CsALAS-driven C4 pathway or the *hemA*/*hemL*-based C5 pathway individually. Consistently, *Rh*DypB-R80 activity in the combinatorial strain decreased to 0.45 $U \cdot mL^{-1}$, compared with 0.48 $U \cdot mL^{-1}$ in the single CsALAS overexpression strain. These results indicate that simultaneous reinforcement of the two upstream 5-ALA-supply pathways did not produce a synergistic improvement in heme accumulation or *Rh*DypB-R80 activity under the tested conditions. Therefore, further increasing upstream precursor supply alone appeared insufficient to improve heme-dependent *Rh*DypB-R80 activity. This observation is consistent with previous studies suggesting that efficient heme production in engineered *E. coli* requires coordinated regulation of upstream precursor formation and downstream tetrapyrrole conversion steps, rather than reinforcement of upstream modules alone (Pranawidjaja et al. 2015; Zhang et al. 2015; Zhao et al. 2018).

To further examine potential downstream constraints in heme biosynthesis, we divided the pathway into two functional modules based on previous studies (Dailey et al. 2017). Module I contained *hemB*, *hemC*, and *hemD*, and Module II contained *hemE*, *hemF*, *hemG*, and *hemH* (Figure 3a; Feng et al. 2022). The overexpression of Module I resulted in a modest rise in intracellular heme levels, which suggests that early downstream steps were not the main bottleneck. Comparatively, Module II (*hemEFGH* cluster) overexpression resulted in significant increases in heme production, with titers being 3.3-fold greater than those achieved with Module I. Peroxidase activity showed the same trend, confirming that reactions encoded by *hemE-hemH* represented the major bottleneck under fermentation conditions (Figure 3b).

Based on these results, we constructed a strain co-expressing CsALAS together with *hemA*, *hemL*, and the *hemEFGH* genes to increase intracellular heme availability. Although total intracellular heme level decreased slightly, likely reflecting metabolic burden during multi-gene expression, the enzyme activity of *Rh*DypB-R80 increased markedly, reaching 0.58 $U \cdot mL^{-1}$. The engineered strain displayed enzyme activity comparable to that obtained with exogenous heme supplementation, indicating that reinforced endogenous heme biosynthesis can sustain catalytic performance without the need for external hemin addition. Consistently, the estimated heme incorporation level of purified *Rh*DypB-R80 was also increased in the final engineered strain (Supporting Information S1: Figure S2).

3.4 | Catalytic Characteristics and Mycotoxin Degradation of *Rh*DypB-R80

ABTS was employed as a model substrate for routine enzymatic activity assays of *Rh*DypB-R80. Using this assay, we systematically investigated the effects of pH, temperature, and the concentrations of H_2O_2 and Mn^{2+} to identify optimal reaction parameters for subsequent enzymatic property characterization.

The optimal pH was determined at 25°C in malonate buffer over a pH range from 3.0 to 8.0. As shown in Figure 4a, *Rh*DypB-R80 showed its highest activity under mildly acidic conditions. The specific activity increased as the pH rose from 3.0 to 5.0, reaching a maximum of 14.91 $U \cdot mg^{-1}$ at pH 5.0, whereas activity declined sharply above pH 6.0, decreasing to 8.04 $U \cdot mg^{-1}$, indicating a marked loss of catalytic efficiency under near-neutral conditions. This acidic optimum is likely related to protonation changes around the heme pocket that affect substrate binding and catalytic turnover in DyPs (Linde et al. 2015). The effect of temperature on enzyme activity was further examined (Figure 4b). *Rh*DypB-R80 displayed the highest activity at 20°C, whereas activity dropped to nearly 50% of the maximum at 40°C. This result indicates that the enzyme is moderately sensitive to heat and loses most activity at higher temperatures. Apart from pH and temperature, H_2O_2 and Mn^{2+} were also important factors influencing the catalytic activity of *Rh*DypB-R80. As the concentration of H_2O_2 increased, the activity of *Rh*DypB-R80 increased initially and then decreased (Figure 4c). The highest specific activity (19.14 $U \cdot mg^{-1}$) was obtained at 0.2 mM H_2O_2, whereas activity declined to 14.50 and 10.77 $U \cdot mg^{-1}$ at 1.0 and 2.0 mM, respectively, suggesting partial oxidative inactivation at high peroxide levels. Similar peroxide-induced inactivation of DyP enzymes has been reported for the DyP from basidiomycete *Pleurotus sapidus* (Avram et al. 2018). The effect of Mn^{2+} concentration was further examined (Figure 4d). In the absence of Mn^{2+}, *Rh*DypB-R80 still retained considerable activity (15.34 $U \cdot mg^{-1}$), suggesting that Mn^{2+} was not essential for ABTS oxidation. However, Mn^{2+} supplementation slightly enhanced catalytic efficiency, and activity remained relatively stable within 0.4-0.8 mM and peaked at 0.6 mM. At 1.0 mM, activity declined slightly, possibly due to nonspecific ionic effects or partial inhibition at elevated metal concentrations. These results suggest that Mn^{2+} acts as a weak enhancer rather than an essential cofactor for *Rh*DypB-R80 (Roberts et al. 2011; Singh and Eltis 2015). Under the optimized conditions of 20°C, pH 5.0, 0.2 mM H_2O_2, and 0.6 mM Mn^{2+}, the enzyme reached a maximum specific activity of 19.81 $U \cdot mg^{-1}$. After determining the catalytic properties of *Rh*DypB-R80 with ABTS as a model substrate, its ability to degrade AFB_1 was subsequently tested. At pH 5.0 and 20°C with 0.6 mM $MnSO_4$ and 0.2 mM H_2O_2, *Rh*DypB-R80 achieved 91.03% AFB_1 removal within 24 h (Supporting Information S1: Figure S3). The structural basis for this efficient detoxification was further supported by molecular dynamics (MD) simulations (Supporting Information S1: Figure S4).

These results identified the optimal reaction conditions for *Rh*DypB-R80, with maximal activity observed under acidic condications and a moderate enhancement in the presence of Mn^{2+}. Beyond ABTS oxidation, *Rh*DypB-R80 also showed effective degradation of AFB_1, supporting its potential

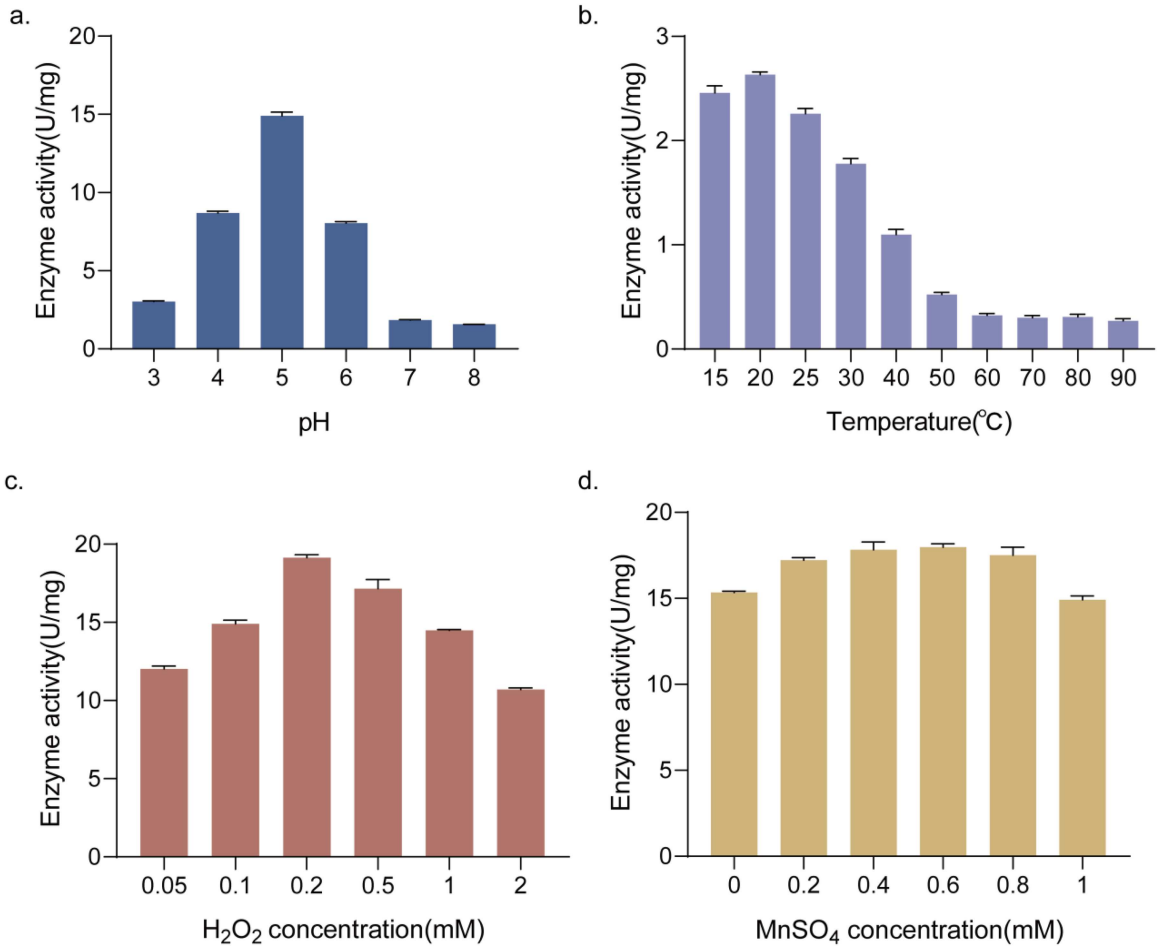

FIGURE 4 | Optimization of catalytic conditions for ABTS oxidation by *Rh*DypB-R80. (a) Effect of pH on enzymatic activity. (b) Effect of temperature on enzymatic activity. (c) Effect of H_2O_2 concentration on enzymatic activity. (d) Effect of $MnSO_4$ concentration on enzymatic activity. Data are presented as the mean ± SD ($n = 3$).

application in the enzymatic control of mycotoxin contamination. The biochemical stability and functional versatility exhibited by *Rh*DypB-R80 support its potential as a promising biocatalyst for industrial mycotoxin detoxification, offering a sustainable solution for food and feed safety (Liu et al. 2024).

4 | Conclusion

The effective expression of the heme-dependent enzymes in microbial hosts is still a problem since the availability of intracellular heme tends to limit the production of catalytically competent holoproteins. Inadequate heme supply in the *Rh*DypB-R80 peroxidase system resulted in the formation of inactive apoenzymes and a decrease in catalytic activity (Choby and Skaar 2016; Layer et al. 2010). In order to overcome this constraint, we redesigned host cofactor metabolism. As demonstrated by transporter engineering, expression of the *E. coli*-derived ChuA transporter resulted in better functional enzyme production than the heterologous PhuR system, which emphasizes the significance of compatibility with the endogenous TonB complex in mediating efficient heme uptake and utilization (Noinaj et al. 2010).

Reconstruction of the heme biosynthetic pathway also suggested that steady-state heme levels were not raised by enhancing upstream precursor supply alone. Upstream reaction improvement was metabolically demanding and failed to enhance enzyme activity. Conversely, coordinated modulation of downstream processes enhanced conversion efficiency, indicating that effective cofactor provision depends on balanced pathway regulation, as opposed to mere amplification of initial reactions (Ajikumar et al. 2010). This observation offers a viable framework to enhance the expression of other heme-dependent enzymes in microbial chassis (Layer et al. 2010).

Following optimization, recombinant *Rh*DypB-R80 exhibited pronounced peroxidase activity against ABTS, with optimal activity achieved under slightly acidic conditions. In another degradation test using aflatoxin B_1 as substrate, the engineered enzyme attained over 90% toxin elimination within 24 h, proving that the engineered enzyme could degrade toxins under the tested condition. In the content of food applications, aflatoxin contamination is prevalent in grains, including maize, peanuts, and other cereal-based products during storage and processing. The reported degradation efficiency means that the optimized enzyme system may have potential for use in post-harvest detoxification efforts, such as treatment of contaminated lots of grain, inclusion in feed processing, or incorporation into fermentation-based grain stabilization efforts. Since the reaction conditions applied in this study can function in mildly acidic

conditions that are typically present during grain preservation and fermentation, it may have potential to be incorporated into current processing steps.

This study shows that with targeted modulation of host heme metabolism it is possible to overcome the bottleneck in recombinant peroxidase expression and offers a broadly applicable method of devising effective enzyme-based approaches to mycotoxin mitigation in food and feed systems.

Author Contributions

Yue Sun: writing – original draft. **Jin-Ping Chen:** data curation. **Nan-Kai Wang:** data curation. **Chang Su:** writing – review and editing. **Heng Li:** writing – review and editing. **Jin-Song Gong:** writing – original draft. **Zheng-Hong Xu:** supervision. **Jin-Song Shi:** supervision.

Acknowledgments

This work was financially supported by the National Key Research and Development Program of China (No. 2024YFA0917900), the Taishan Industry Leading Talent of Shandong Province (No. tscx202408107), the Open Project Foundation in Key Laboratory of Carbohydrate Chemistry and Biotechnology of Ministry of Education (No. KLCCB-KF202510) and the Major Scientific and Technological Project in the Inner Mongolia Autonomous Region.

Ethic Statement

The authors have nothing to report.

Conflicts of Interest

The authors declare no conflicts of interest.

Data Availability Statement

The data that support the findings of this study are available from the corresponding author upon reasonable request.

References

Ajikumar, P. K., W. H. Xiao, K. E. J. Tyo, et al. 2010. "Isoprenoid Pathway Optimization for Taxol Precursor Overproduction in *Escherichia coli*." *Science* 330, no. 6000: 70–74. https://doi.org/10.1126/science.1191652.

Andrews, S. C., A. K. Robinson, and F. Rodríguez-Quiñones. 2003. "Bacterial Iron Homeostasis." *FEMS Microbiology Reviews* 27, no. 2/3: 215–237. https://doi.org/10.1016/S0168-6445(03)00055-X.

Avram, A., A. Sengupta, P. H. Pfromm, et al. 2018. "Novel DyP From the Basidiomycete *Pleurotus sapidus*: Substrate Screening and Kinetics." *Biocatalysis* 4, no. 1: 1–13. https://doi.org/10.1515/boca-2018-0001.

Barr, I., and F. Guo. 2015. "Pyridine Hemochromagen Assay for Determining the Concentration of Heme in Purified Protein Solutions." *Bio-Protocol* 5, no. 18: 1594. https://doi.org/10.21769/bioprotoc.1594.

Bullerman, L. B., and A. Bianchini. 2007. "Stability of Mycotoxins During Food Processing." *International Journal of Food Microbiology* 119, no. 1/2: 140–146. https://doi.org/10.1016/j.ijfoodmicro.2007.07.035.

Chan, A. C. K., B. Lelj-Garolla, F. I. Rosell, K. A. Pedersen, A. G. Mauk, and M. E. P. Murphy. 2006. "Cofacial Heme Binding Is Linked to Dimerization by a Bacterial Heme Transport Protein." *Journal of Molecular Biology* 362, no. 5: 1108–1119. https://doi.org/10.1016/j.jmb.2006.08.001.

Choby, J. E., and E. P. Skaar. 2016. "Heme Synthesis and Acquisition in Bacterial Pathogens." *Journal of Molecular Biology* 428, no. 17: 3408–3428. https://doi.org/10.1016/j.jmb.2016.03.018.

Dailey, H. A., T. A. Dailey, S. Gerdes, et al. 2017. "Prokaryotic Heme Biosynthesis: Multiple Pathways to a Common Essential Product." *Microbiology and Molecular Biology Reviews* 81, no. 1: 00048–00016. https://doi.org/10.1128/MMBR.00048-16.

Diao, E., H. Hou, W. Hu, et al. 2018. "Removing and Detoxifying Methods of Patulin: A Review." *Trends in Food Science & Technology* 81: 139–145. https://doi.org/10.1016/j.tifs.2018.09.016.

Du, X., M. Zheng, H. Zhang, et al. 2025. "New Application of a Dye-Decolorizing Peroxidase Immobilized on Magnetic Nanoparticles for Efficient Simultaneous Degradation of Two Mycotoxins." *Food Chemistry* 463, no. pt. 2: 141341. https://doi.org/10.1016/j.foodchem.2024.141341.

Eskola, M., G. Kos, C. T. Elliott, J. Hajšlová, S. Mayar, and R. Krska. 2020. "Worldwide Contamination of Food-Crops With Mycotoxins: Validity of the Widely Cited 'FAO Estimate' of 25%." *Critical Reviews in Food Science and Nutrition* 60, no. 16: 2773–2789. https://doi.org/10.1080/10408398.2019.1658570.

Feng, C., M. Pan, and L. Tang. 2022. "5-Aminolevulinic Acid Level and Dye-Decolorizing Peroxidase Expression Regulate Heme Synthesis in *Escherichia coli*." *Biotechnology Letters* 44, no. 2: 271–277. https://doi.org/10.1007/s10529-021-03212-z.

Fiege, K., C. J. Querebillo, P. Hildebrandt, and N. Frankenberg-Dinkel. 2018. "Improved Method for the Incorporation of Heme Cofactors Into Recombinant Proteins Using *Escherichia coli* Nissle 1917." *Biochemistry* 57, no. 19: 2747–2755. https://doi.org/10.1021/acs.biochem.8b00242.

Ge, J., X. Wang, Y. Bai, et al. 2023. "Engineering *Escherichia coli* for Efficient Assembly of Heme Proteins." *Microbial Cell Factories* 22, no. 1: 59. https://doi.org/10.1186/s12934-023-02067-5.

Harnastai, I. N., A. A. Gilep, and S. A. Usanov. 2006. "The Development of an Efficient System for Heterologous Expression of Cytochrome P450s in *Escherichia coli* Using *hemA* Gene Co-Expression." *Protein Expression and Purification* 46, no. 1: 47–55. https://doi.org/10.1016/j.pep.2005.07.006.

Hofrichter, M. 2002. "Review: Lignin Conversion by Manganese Peroxidase (MnP)." *Enzyme and Microbial Technology* 30, no. 4: 454–466. https://doi.org/10.1016/S0141-0229(01)00528-2.

Hu, B., H. Yu, J. Zhou, et al. 2023. "Whole-Cell P450 Biocatalysis Using Engineered *Escherichia coli* With Fine-Tuned Heme Biosynthesis." *Advanced science (Weinheim, Baden-Wurttemberg, Germany)* 10, no. 6: 2205580. https://doi.org/10.1002/advs.202205580.

Kato, S., M. Abe, N. Okahashi, et al. 2025. "Metabolic Engineering of the 5-Aminolevulinate Biosynthetic Pathway in *E. coli* Improves Efficiency of Hemoprotein-Based Biocatalysis." *Angewandte Chemie International Edition* 64, no. 39: 202512156. https://doi.org/10.1002/anie.202512156.

Khan, R., F. Anwar, and F. M. Ghazali. 2024. "A Comprehensive Review of Mycotoxins: Toxicology, Detection, and Effective Mitigation Approaches." *Heliyon* 10, no. 8: e28361. https://doi.org/10.1016/j.heliyon.2024.e28361.

Ko, Y. J., M. Kim, S. K. You, et al. 2021. "Animal-Free Heme Production for Artificial Meat in *Corynebacterium glutamicum* via Systems Metabolic and Membrane Engineering." *Metabolic Engineering* 66: 217–228. https://doi.org/10.1016/j.ymben.2021.04.013.

Layer, G. 2021. "Heme Biosynthesis in Prokaryotes." *Biochimica et Biophysica Acta, Molecular Cell Research* 1868, no. 1: 118861. https://doi.org/10.1016/j.bbamcr.2020.118861.

Layer, G., J. Reichelt, D. Jahn, and D. W. Heinz. 2010. "Structure and Function of Enzymes in Heme Biosynthesis." *Protein Science* 19, no. 6: 1137–1161. https://doi.org/10.1002/pro.405.

Linde, D., F. J. Ruiz-Dueñas, E. Fernández-Fueyo, et al. 2015. "Basidiomycete DyPs: Genomic Diversity, Structural-Functional Aspects, Reaction Mechanism and Environmental Significance." *Archives of Biochemistry and Biophysics* 574: 66–74. https://doi.org/10.1016/j.abb.2015.01.018.

Liu, M., X. Zhang, H. Luan, et al. 2024. "Bioenzymatic Detoxification of Mycotoxins." *Frontiers in Microbiology* 15: 1434987. https://doi.org/10.3389/fmicb.2024.1434987.

Loi, M., J. B. Renaud, E. Rosini, et al. 2020. "Enzymatic Transformation of Aflatoxin B_1 by Rh_DypB Peroxidase and Characterization of the Reaction Products." *Chemosphere* 250: 126296. https://doi.org/10.1016/j.chemosphere.2020.126296.

Mafe, A. N., and D. Büsselberg. 2024. "Mycotoxins in Food: Cancer Risks and Strategies for Control." *Foods* 13, no. 21: 3502. https://doi.org/10.3390/foods13213502.

Marvig, R. L., S. Damkiær, S. M. H. Khademi, T. M. Markussen, S. Molin, and L. Jelsbak. 2014. "Within-Host Evolution of *Pseudomonas aeruginosa* Reveals Adaptation Toward Iron Acquisition From Hemoglobin." *mBio* 5, no. 3: e00966–00914. https://doi.org/10.1128/mBio.00966-14.

Mota, M. N., M. Palma, and I. Sá-Correia. 2024. "*Candida boidinii* Isolates From Olive Curation Water: A Promising Platform for Methanol-Based Biomanufacturing." *AMB Express* 14, no. 1: 93. https://doi.org/10.1186/s13568-024-01754-9.

Noinaj, N., M. Guillier, T. J. Barnard, and S. K. Buchanan. 2010. "TonB-Dependent Transporters: Regulation, Structure, and Function." *Annual Review of Microbiology* 64: 43–60. https://doi.org/10.1146/annurev.micro.112408.134247.

Pérez-Pérez, J., and J. Gutiérrez. 1995. "An Arabinose-Inducible Expression Vector, pAR3, Compatible With ColE1-Derived Plasmids." *Gene* 158, no. 1: 141–142. https://doi.org/10.1016/0378-1119(95)00127-r.

Pfanzagl, V., M. Bellei, S. Hofbauer, et al. 2019. "Redox Thermodynamics of B-Class Dye-Decolorizing Peroxidases." *Journal of Inorganic Biochemistry* 199: 110761. https://doi.org/10.1016/j.jinorgbio.2019.110761.

Pranawidjaja, S., S. I. Choi, B. W. Lay, and P. Kim. 2015. "Analysis of Heme Biosynthetic Pathways in a Recombinant *Escherichia coli*." *Journal of Microbiology and Biotechnology* 25, no. 6: 880–886. https://doi.org/10.4014/jmb.1411.11050.

Roberts, J. N., R. Singh, J. C. Grigg, M. E. P. Murphy, T. D. H. Bugg, and L. D. Eltis. 2011. "Characterization of Dye-Decolorizing Peroxidases From *Rhodococcus jostii* RHA1." *Biochemistry* 50, no. 23: 5108–5119. https://doi.org/10.1021/bi200427h.

Singh, R., and L. D. Eltis. 2015. "The Multihued Palette of Dye-Decolorizing Peroxidases." *Archives of Biochemistry and Biophysics* 574: 56–65. https://doi.org/10.1016/j.abb.2015.01.014.

Singh, R., J. C. Grigg, W. Qin, J. F. Kadla, M. E. P. Murphy, and L. D. Eltis. 2013. "Improved Manganese-Oxidizing Activity of DypB, a Peroxidase From a Lignolytic Bacterium." *ACS Chemical Biology* 8, no. 4: 700–706. https://doi.org/10.1021/cb300608x.

Strittmatter, E., C. Liers, R. Ullrich, et al. 2013. "First Crystal Structure of a Fungal High-Redox Potential Dye-Decolorizing Peroxidase." *Journal of Biological Chemistry* 288, no. 6: 4095–4102. https://doi.org/10.1074/jbc.M112.400176.

Sugano, Y., R. Muramatsu, A. Ichiyanagi, T. Sato, and M. Shoda. 2007. "DyP, a Unique Dye-Decolorizing Peroxidase, Represents a Novel Heme Peroxidase Family." *Journal of Biological Chemistry* 282, no. 50: 36652–36658. https://doi.org/10.1074/jbc.M706996200.

Wang, J., M. Ogata, H. Hirai, and H. Kawagishi. 2011. "Detoxification of Aflatoxin B_1 by Manganese Peroxidase From the White-Rot Fungus *Phanerochaete sordida* YK-624." *FEMS Microbiology Letters* 314, no. 2: 164–169. https://doi.org/10.1111/j.1574-6968.2010.02158.x.

Wang, X., X. Qin, Z. Hao, H. Luo, B. Yao, and X. Su. 2019. "Degradation of Four Major Mycotoxins by Eight Manganese Peroxidases in Presence of a Dicarboxylic Acid." *Toxins* 11, no. 10: 566. https://doi.org/10.3390/toxins11100566.

Xu, H., L. Wang, J. Sun, et al. 2022. "Microbial Detoxification of Mycotoxins in Food and Feed." *Critical Reviews in Food Science and Nutrition* 62, no. 18: 4951–4969. https://doi.org/10.1080/10408398.2021.1879730.

Yu, F., Z. Wang, Z. Zhang, et al. 2024. "Biosynthesis, Acquisition, Regulation, and Upcycling of Heme: Recent Advances." *Critical Reviews in Biotechnology* 44, no. 7: 1422–1438. https://doi.org/10.1080/07388551.2023.2291339.

Zámocký, M., S. Hofbauer, I. Schaffner, et al. 2015. "Independent Evolution of Four Heme Peroxidase Superfamilies." *Archives of Biochemistry and Biophysics* 574: 108–119. https://doi.org/10.1016/j.abb.2014.12.025.

Zhang, J., Z. Kang, J. Chen, and G. Du. 2015. "Optimization of the Heme Biosynthesis Pathway for the Production of 5-aminolevulinic Acid in *Escherichia coli*." *Scientific Reports* 5: 8584. https://doi.org/10.1038/srep08584.

Zhao, X. R., K. R. Choi, and S. Y. Lee. 2018. "Metabolic Engineering of *Escherichia coli* for Secretory Production of Free Haem." *Nature Catalysis* 1, no. 9: 720–728. https://doi.org/10.1038/s41929-018-0126-1.

Supporting Information

Additional supporting information can be found online in the Supporting Information section.

Supporting File: fbe270063-sup-0001-20260506-05_29Supplementary_Information.docx.